Diabetes-Induced Cellular Senescence and Senescence-Associated Secretory Phenotype Impair Cardiac Regeneration and Function Independently of Age

Fabiola Marino,[1,2] Mariangela Scalise,[1] Nadia Salerno,[3] Luca Salerno,[1] Claudia Molinaro,[3] Donato Cappetta,[4] Michele Torella,[5] Marta Greco,[6] Daniela Foti,[1] Ferdinando C. Sasso,[5] Pasquale Mastroroberto,[1] Antonella De Angelis,[4] Georgina M. Ellison-Hughes,[7] Maurilio Sampaolesi,[2] Marcello Rota,[8] Francesco Rossi,[4] Konrad Urbanek,[1] Bernardo Nadal-Ginard,[3] Daniele Torella,[1] and Eleonora Cianflone[3,8]

Diabetes 2022;71:1081–1098 | https://doi.org/10.2337/db21-0536

Diabetes mellitus (DM) affects the biology of multipotent cardiac stem/progenitor cells (CSCs) and adult myocardial regeneration. We assessed the hypothesis that senescence and senescence-associated secretory phenotype (SASP) are main mechanisms of cardiac degenerative defect in DM. Accordingly, we tested whether ablation of senescent CSCs would rescue the cardiac regenerative/reparative defect imposed by DM. We obtained cardiac tissue from nonaged (50- to 64-year-old) patients with type 2 diabetes mellitus (T2DM) and without DM (NDM) and postinfarct cardiomyopathy undergoing cardiac surgery. A higher reactive oxygen species production in T2DM was associated with an increased number of senescent/dysfunctional T2DM-human CSCs (hCSCs) with reduced proliferation, clonogenesis/spherogenesis, and myogenic differentiation versus NDM-hCSCs in vitro. T2DM-hCSCs showed a defined pathologic SASP. A combination of two senolytics, dasatinib (D) and quercetin (Q), cleared senescent T2DM-hCSCs in vitro, restoring their expansion and myogenic differentiation capacities. In a T2DM model in young mice, diabetic status per se (independently of ischemia and age) caused CSC senescence coupled with myocardial pathologic remodeling and cardiac dysfunction. D + Q treatment efficiently eliminated senescent cells, rescuing CSC function, which resulted in functional myocardial repair/regeneration, improving cardiac function in murine DM. In conclusion, DM hampers CSC biology, inhibiting CSCs' regenerative potential through the induction of cellular senescence and SASP independently from aging. Senolytics clear senescence, abrogating the SASP and restoring a fully proliferative/differentiation-competent hCSC pool in T2DM with normalization of cardiac function.

Aging is a major risk factor for the occurrence of several diseases, including stroke, myocardial infarction, heart failure (HF), neurodegenerative disease, and several cancers. Therefore, the global rise in life expectancy will lead to a

[1]Department of Experimental and Clinical Medicine, Magna Græcia University, Catanzaro, Italy
[2]Translational Cardiomyology Laboratory, Stem Cell Biology and Embryology, Department of Development and Regeneration, KU Leuven, Leuven, Belgium
[3]Department of Medical and Surgical Sciences, Magna Græcia University, Catanzaro, Italy
[4]Department of Experimental Medicine, Section of Pharmacology, University of Campania "L. Vanvitelli," Naples, Italy
[5]Department of Translational Medicine, University of Campania "L. Vanvitelli," Naples, Italy
[6]Department of Health Sciences, Magna Græcia University, Catanzaro, Italy
[7]Centre for Human and Applied Physiological Sciences and Centre for Stem Cells and Regenerative Medicine, School of Basic and Medical Biosciences, Faculty of Life Sciences and Medicine, King's College London, London, U.K.
[8]Department of Physiology, New York Medical College, Valhalla, NY

Corresponding authors: Daniele Torella, dtorella@unicz.it, and Eleonora Cianflone, cianflone@unicz.it

Received 23 June 2021 and accepted 30 January 2022

This article contains supplementary material online at https://doi.org/10.2337/figshare.19098803.

F.M. and M.Sc. contributed equally to this study.

dramatic increase in age-related diseases in the coming decades. In this scenario, cardiovascular diseases, including atherosclerosis and HF, increase exponentially with age, whereby HF is considered an epidemic because of a growing and aging population. Type 2 diabetes mellitus (T2DM) is closely associated with aging and is a powerful independent risk factor for cardiovascular diseases, such as atherosclerosis and HF (1). This epidemiological connection among aging, T2DM, and cardiovascular disease is postulated to be pathophysiologically linked.

Aging has been associated with systemic inflammation and oxidative stress (2), which can be both a cause and a consequence of diabetes mellitus (DM) (3). Cellular senescence can be defined as a permanent arrest of cellular growth and is a key feature of aging (4,5). Cell senescence is also a cause and a consequence of DM and plays an important role in its cardiovascular complications. Although senescent cells are classically reported as cells that irreversibly cease proliferation, they have the capacity to produce and secrete soluble factors that can influence neighboring cells and tissues (6,7). This feature of senescent cells to secrete these soluble factors is called senescence-associated secretory phenotype (SASP) (8). Since chronic inflammation is an important pathophysiologic factor of both aging and DM, SASP has been postulated to be the pathophysiologic link between aging and DM in cardiovascular diseases (9).

Tissue-specific adult stem cell senescence has emerged as an attractive theory for the decline in mammalian tissue and organ function during aging (10). The mammalian heart, including in humans, harbors a tissue-specific cardiac stem/progenitor cell (CSC) compartment (11–15) that undergoes senescence with age, which dictates a progressive and permanent dysfunction of more than one-half of these endogenous cells by 75 years of age (5,10,16,17). The senescent CSCs exhibit an SASP that can negatively affect surrounding cells, causing otherwise healthy and cycling-competent CSCs to lose proliferative capacity and switch to a senescent phenotype. Nevertheless, even at advanced ages, it is still possible to retrieve a healthy, cycling-competent CSC fraction with an effective regenerative and reparative capacity (5,10,16). Accordingly, experimental selective ablation of senescent CSCs either genetically or by a combination of senolytic drugs fosters the expansion and functional regenerative recovery of the healthy aged CSCs (5,10,18).

Several reports have shown that DM impairs the in vitro proliferative and differentiation potential of CSCs (19–21). Changes in chromatin conformation underlie the impaired proliferation, differentiation, and senescent behavior of diabetic CSCs (22). Yet, whether the SASP is induced by DM per se in CSCs and whether targeting senescent cells within the diabetic CSC compartment rescues CSC proliferation and differentiation defect in T2DM is unknown. Therefore, we assessed here the hypothesis that senescence and SASP are main mechanisms of the cardiac degenerative defect in DM. Accordingly, we tested the hypothesis that ablation of senescent CSCs would rescue the cardiac regenerative/reparative defect imposed by DM. We show that the myocardium of patients with T2DM, in a narrow age window of 55–64 years, undergoing cardiac surgery for ischemic heart disease is characterized by an increased oxidative stress that affects the CSC compartment with an increased senescent phenotype compared with myocardium and CSCs of age- and sex-matched patients without DM (NDM). Importantly, T2DM CSCs have an SASP, and senolytic treatment abrogates the senescent diabetic CSCs, which allows healthy CSCs to proliferate and differentiate normally. Using a T2DM model in young mice, we further show that diabetic status per se (independently of ischemia and age) causes CSC senescence coupled with myocardial pathologic remodeling and cardiac dysfunction. Senolytic treatment efficiently eliminates senescent cells, rescuing CSC function, which results in functional myocardial repair/regeneration, improving cardiac function in murine DM.

RESEARCH DESIGN AND METHODS

Patient Cohort and Samples

Human myocardial biopsy specimens were obtained from patients with T2DM and NDM and postinfarct cardiomyopathy undergoing surgical coronary revascularization, as previously described (23). The biopsies were performed by cardiac surgeons in an area immediately adjacent to macroscopically recognized infarcted tissue of the left ventricle (LV). Collection of human tissue samples was approved by the local ethics committee at the University of Campania "L. Vanvitelli" and Magna Græcia University and performed in conformity with the principles outlined in the Declaration of Helsinki. Before cardiac surgery, written informed consent was obtained. All patient data were kept anonymous with no patient identifiers. As inclusion criteria, an age between 55 and 64 years was required in order to try and separate the effects of aging from DM on senescence. We included 10 patients with T2DM and 6 with NDM from whom periinfarct/border zone biopsy specimens were obtained (Supplementary Table 1). Freshly excised samples were formalin fixed for immunohistochemistry analysis as described below. Furthermore, an additional six patients with T2DM and six with NDM with similar characteristics were included (Supplementary Table 1) from whom atrial samples were obtained and processed for cell harvesting. T2DM was defined to be present in patients receiving stable glucose-lowering therapy and having a glycated hemoglobin level of at least 7.0%. NDM status was defined as normal glucose tolerance during a standard oral load glucose test performed before coronary surgery.

Human CSC Isolation and Culture

The c-kit^{pos}CD45^{neg}CD31^{neg} human CSCs (hCSCs) and mouse CSCs (mCSCs) were obtained as previously described (12,15) and plated in CELLstart (Life Technologies) or gelatin-coated dishes in complete CSC growth medium assembled as previously described (12,15). For senolytic treatment,

dasatinib (LC Laboratories) and quercetin (Sigma-Aldrich) were used (5).

Animals

All animal experimental procedures were approved by Magna Græcia institutional review boards on animal use and welfare. Mice were housed under controlled conditions of 25°C, 50% relative humidity, and 12-h light (0600–1800 h) and 12-h dark (1800–0600 h) cycles, with water and food (containing 18.5% protein) available ad libitum, except for the high-fat diet (HFD) (D12492; Research Diets), which is described below. Before any invasive procedure, mice were anesthetized by i.p. injections of tiletamine/zolazepam (80 mg/kg) or inhaled isoflurane (isoflurane 1.5%, oxygen 98.5%, Iso-Vet; Piramal Healthcare).

To induce T2DM in young mice, 6-week-old male and female C57BL/6J mice (Charles River Laboratories) were fed a 60 kcal% HFD for 2 weeks. During the third week, mice received four consecutive daily injections of low-dose streptozotocin (STZ) (40 mg/kg i.p.) dissolved in 0.05 mol/L citrate buffer (pH 4) (24,25). Control mice were fed normal chow diet (NCD) or HFD without STZ. At 8 weeks of the experimental design, diabetic mice were randomly assigned to a dasatinib (5 mg/kg) + quercetin (50 mg/kg) senolytic combination (D + Q) treatment (three consecutive daily i.p. injections every week) or just placebo (vehicle) i.p. injection for 4 weeks. For the latter, D + Q was diluted in vehicle (50% PBS, 20% DMSO, and 30% polyethylene glycol 400). Additional vehicle-treated and D + Q–treated diabetic mice were implanted subcutaneously (between the scapulae) with osmotic minipumps (ALZET) to systemically release BrdU (50 mg/kg/day) for 28 days (15). After 4 weeks, mice were sacrificed and their hearts processed either for immunohistochemistry analysis or for CSC isolation. The complete in vivo animal study design with number of animals for each group is reported in Supplementary Fig. 2.

Echocardiography

Echocardiography analysis was performed using a Vevo 3100 imaging system (FUJIFILM Visualsonics, Inc.), as previously reported (26).

Histology and Immunohistochemistry

Human and mouse tissue specimens were fixed and embedded in paraffin or in optimal cutting temperature compound for immunohistochemical analysis (5,12). Sections were stained with the specific antibodies listed in Supplementary Table 2. Sections were examined by confocal microscopy (Leica TCS SP8).

Immunohistochemical analysis of oxidative stress was performed using the specific antibodies listed in Supplementary Table 2. The positive reactions were visualized using a labeled polymer-horseradish peroxidase complex and 3,3′-diaminobenzidine tetrahydrochloride chromogen (EnVision+ Dual Link System-HRP; DAKO). Sections were then counterstained with hematoxylin and examined with light microscopy (DMI3000B; Leica). For evaluation of fibrosis, Picrosirius Red (Bio-Optica) staining was performed according to the manufacturing instructions.

FACS Analysis

Cell analysis was performed on a BD FACSCanto II running FlowJo software (Tree Star) to identify the percentage of cardiac small cells expressing different cell surface markers (12). Specific antibodies used are listed in Supplementary Table 2. Reactive oxygen species (ROS) generation was determined using a CellROX Flow Cytometry Assay Kit (Life Technologies) according to the manufacturing instructions.

Proliferation, Clonogenicity, Cardiosphere Formation, and Cardiomyocyte Differentiation Assays In Vitro

Proliferation of hCSCs and mCSCs were evaluated through BrdU incorporation (10 μmol/L; Roche) and growth curve assays (5,12). Single-cell cloning was used through depositing a half-cell per well into 96-well CELLstart-coated Terasaki plates (12). For cardiosphere generation, 1×10^5 hCSCs and mCSCs were placed in extra-low-attachment dishes in CSC growth medium (12).

For specific myogenic differentiation, hCSC- and mCSC-derived cardiospheres were placed in bacteriological dishes for 5–7 days for cardiosphere generation in CSC growth medium. Cardiospheres were then switched to base differentiation medium consisting of StemPro-34 SFM (a serum-free medium conditioned with StemPro-Nutrient Supplement; Gibco, Life Technologies), glutamine (2 mmol/L), and penicillin-streptomycin (1%; Life Technologies) (12,27). For specific myocyte differentiation, BMP4 (10 ng/mL; Peprotech), activin A (10 ng/mL first day and then 5 ng/mL; Peprotech), β-fibroblast growth factor (10 ng/mL; Peprotech), Wnt-11 (150 ng/mL; R&D Systems), and Wnt-5a (150 ng/mL, R&D Systems) were added to base differentiation medium from day 0 to day 4. At day 4, differentiating cardiospheres were pelleted and transferred to dishes coated with laminin (1 μg/mL), and Dkk-1 (150 ng/mL; R&D Systems) was added to base differentiation medium from day 5 to day 14 (12,27). Differentiated mCSCs were trypsinized for RNA isolation.

From day 15 to day 28, the base differentiation medium for hCSCs were replaced by Gibco PSC Cardiomyocyte Differentiation Media (A2921201; Thermo Fisher Scientific), and differentiated cardiomyocyte–derived hCSCs were then either trypsinized for RNA isolation or fixed with 4% paraformaldehyde (#P6148; Sigma-Aldrich) and stained for cardiac troponin I (cTnI) and actinin.

Immunocytochemistry

A volume of 200 μL of a 0.15×10^6 cells/mL suspension of CSCs was cytospun using a Shandon Cytospin 4 Cytocentrifuge (Thermo Fisher Scientific). Slides were immediately fixed using 4% paraformaldehyde (Sigma-Aldrich). After

fixation, specific antibodies were used (5) (Supplementary Table 2).

Telomere Length and Telomerase Activity Quantification

Genomic DNA of T2DM-hCSCs and NDM-hCSCs was extracted using Quick-DNA Microprep Kit (Zymo Research). Telomere length was analyzed by using the Absolute Human Telomere Length Quantification qPCR Assay Kit (ScienCell Research Laboratories) (12). T2DM-hCSCs and NDM-hCSCs were processed using the Telomerase Activity Quantification qPCR Assay Kit (ScienCell Research Laboratories) (12,28).

RNA Extraction and RT-PCR Analysis

RNA was extracted from T2DM-hCSCs and NDM-hCSCs, mCSCs isolated from vehicle or D + Q–treated diabetic mice, and control mice using TRIzol (Ambion). Reverse transcription was performed with 1–2 μg of RNA using High-Capacity cDNA Kit (Applied Biosystems). Quantitative RT-PCR (qRT-PCR) was performed using TaqMan primer and probe sets (see Supplementary Table 3) using a StepOnePlus Real-Time PCR System (Applied Biosystems).

Western Blot Analysis

Immunoblots were performed using protein lysates obtained from T2DM-hCSCs and NDM-hCSCs as previously described (23). The relative antibodies are listed in Supplementary Table 2.

Cytokine and Growth Factor Assay

Cytokine and growth factor levels were simultaneously evaluated using a cytokine and growth factors array kit (CTK; Randox Laboratories) with an Evidence Investigator biochip analyzer (Randox Laboratories) (29).

Statistical Analysis

All data are presented as mean ± SD. Data were analyzed using *t* test comparisons in GraphPad Prism 8.0.0 for Windows (GraphPad Software, San Diego, CA). Differences of $P < 0.05$ are considered statistically significant.

Data and Resource Availability

All data generated or analyzed during this study are included in the published article and its online supplementary files.

RESULTS

Increased Oxidative Stress in Diabetic Ischemic Cardiomyopathy

DM is characterized by an enhanced oxygen toxicity (30). ROS is the distal signal of the cascade of events triggered by DM that leads to the initiation of the cell death pathway in the heart (31). Human samples were thus analyzed for the presence of 8-hydroxy-deoxyguanosine (8-OH-dG), nitrotyrosine (3-NT), and 4-hydroxinonenal (4-HNE). Patients with T2DM exhibited an increase of myocardial cells positive for these markers of oxidative stress compared with patients with NDM (Fig. 1*A*–*C*). In particular, a higher percentage of both cardiomyocytes and CSC-enriched c-kit^{pos}CD45^{neg}CD31^{neg} cardiac cells positive for 8-OH-dG and 3-NT were detected in T2DM compared with NDM (Fig. 2*A* and *B*). These data show that cardiac damage in T2DM is associated with a higher ROS production that targets both muscle cells and adult progenitor cells.

Increased Oxidative Stress Associated With Increased Expression of Senescent Markers in hCSCs from Diabetic Ischemic Cardiomyopathy

Cellular senescence is a cell state triggered by stressful insults and certain physiological processes characterized by a prolonged and generally irreversible cell-cycle arrest with secretory features, macromolecular damage, and altered metabolism (32). These alterations are generally interdependently because oxygen toxicity and DNA damage alter telomeres, resulting in telomere shortening, cellular senescence, and cell dysfunction and/or death (32). Although a link to organismal aging is clear, aging and senescence are not synonymous as, indeed, cells can undergo senescence regardless of organismal age (33,34). On the other hand, aging tissues experience a progressive decline in homeostatic and regenerative capacities, which have been attributed to senescence of their tissue-specific stem cells (35). To assess whether the exaggerated ROS in T2DM is associated with senescence of tissue-resident CSCs independently of age, we first assessed the expression of p16^{INK4a} in CSC-enriched c-kit^{pos}CD45^{neg}CD31^{neg} cardiac cells in the myocardial sections from samples obtained from nonaged (55- to 64-year-old) patients with T2DM compared with age-matched patients with NDM. Despite not being sufficient on its own to define/detect senescent cells, p16^{INK4a} is widely used as a senescent biomarker (36–40). The expression of p16^{INK4a} in CSC-enriched c-kit^{pos}CD45^{neg}CD31^{neg} cardiac cells markedly increased in myocardial samples from patients with T2DM and ischemic cardiomyopathy compared with their counterparts with NDM (Fig. 2*C*), confirming that a higher myocardial oxidative stress couples with the induction of senescence in the cardiac progenitor pool.

To further assess senescence in the adult progenitor pool, we established cultures of hCSCs from atrial specimens of patients with T2DM ($n = 6$) and NDM ($n = 6$) undergoing cardiac surgery (Supplementary Table 1). The c-kit^{pos}CD45^{neg}CD31^{neg} cardiac cells from T2DM (hereafter, T2DM-hCSCs) showed a membrane phenotype typical of cardiac cells enriched with multipotent hCSCs (Supplementary Fig. 1*A*), as we have previously shown (12,41,42), with no significant difference compared with c-kit^{pos}CD45^{neg}CD31^{neg} cardiac cells from patients with NDM (hereafter NDM-hCSCs) (data not shown). Briefly, isolated T2DM-hCSCs, except for c-kit and CXCR4, were negative for the main human hematopoietic stem cell markers (namely CD45, CD34, CD38, and CD150). They are instead positive for several mesenchymal stem cell markers like CD90, CD105, CD166, CD73, CD13, CD29,

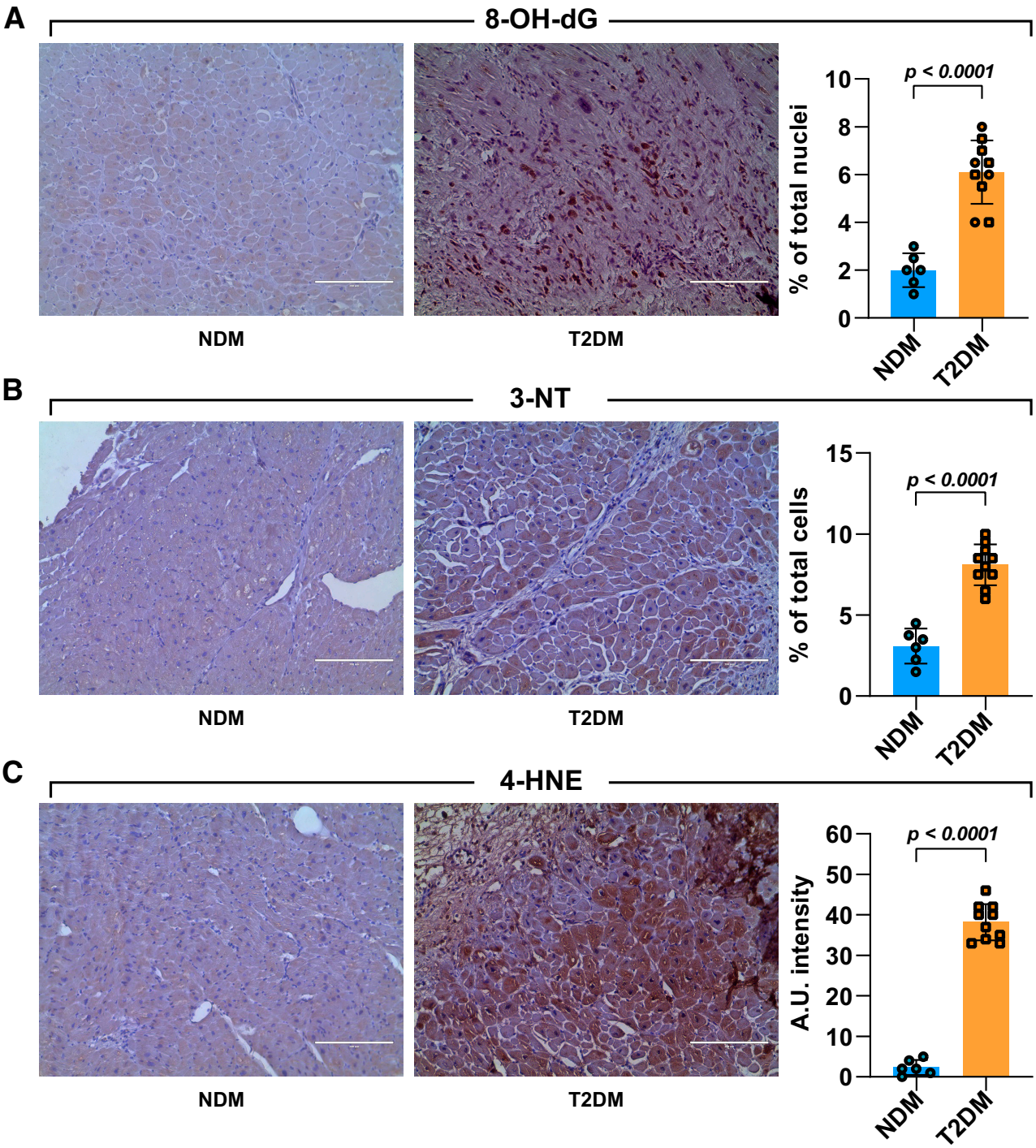

Figure 1—Cardiac damage in diabetes is associated with higher ROS production. *A–C*: Light microscopy images show representative 3,3′-diaminobenzidine tetrahydrochloride staining of LV samples obtained from patients with T2DM and NDM. The respective bar graphs show (in brown) the percentage of 8-OH-dG–positive nuclei (*A*), 3-NT–positive cells (*B*), and the 4-HNE arbitrary unit (A.U.) intensity levels (*C*) in T2DM compared with NDM heart tissue cross sections (n = 10 and 6, respectively). Scale bars = 200 μm. Data are mean ± SD.

CD44, and Stro-1 (Supplementary Fig. 1*A*). A very small fraction of freshly isolated hCSCs also expressed pluripotency markers like OCT4 (2 ± 2%), SOX2 (10 ± 5%), NANOG (15 ± 4%), KLF4 (8 ± 3%), and cMYC (1 ± 1%), and a small cell fraction expressed Sac2 (3 ± 2%) (Supplementary Fig. 1*B*).

In agreement with myocardial tissue assessment, T2DM-hCSCs at the single-cell level showed increased ROS expression compared with NDM-hCSCs (Fig. 3*A*). As first assessment of replicative senescence in the isolated cells, we measured telomerase activity and telomeric length (Fig. 3*B*). T2DM-hCSCs showed a significantly reduced

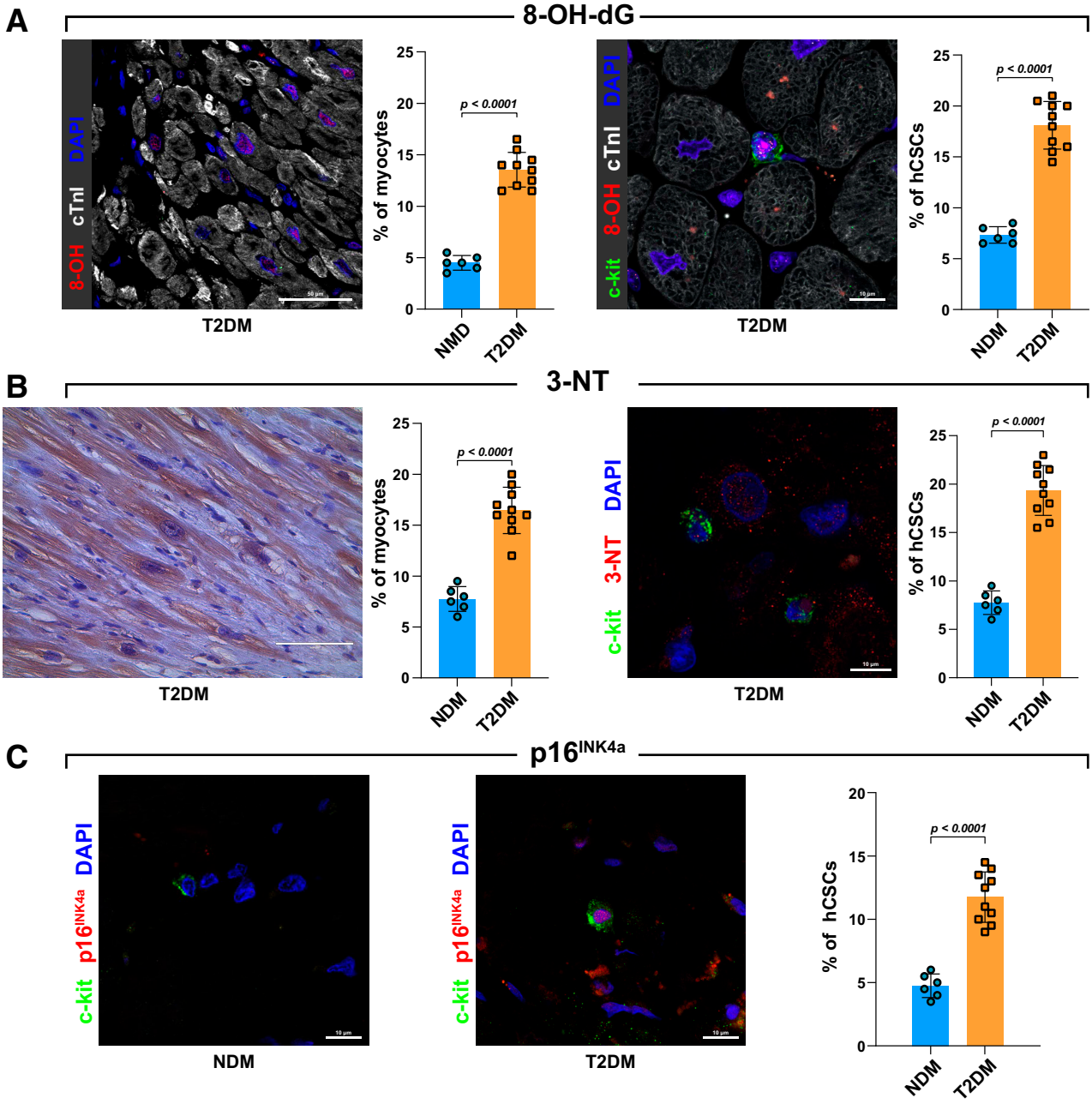

Figure 2—Quantification of oxidative stress and senescent markers in myocytes and progenitor cells. *A*: Representative confocal images and bar graphs showing 8-OH-dG–positive cardiomyocytes and 8-OH-dG–positive hCSCs in LV samples obtained from patients with T2DM (8-OH-dG, red; c-kit, green; cTnI, white; DAPI, blue; $n = 10$ and 6 T2DM and NDM heart sections, respectively). Scale bars = 50 μm and 10 μm, respectively. *B*: Representative light microscopy, confocal image, and bar graphs showing 3-NT–positive cardiomyocytes (brown) and 3-NT–positive hCSCs in LV samples obtained from patients with T2DM and NDM (3-NT, red; c-kit, green; DAPI, blue; $n = 10$ and 6 T2DM and NDM heart sections, respectively). Scale bars = 100 μm and 10 μm, respectively. *C*: Bar graph and representative confocal images showing $p16^{INK4a}$ expression in LV T2DM-hCSCs compared with NDM-hCSCs ($p16^{INK4a}$, red; c-kit, green; DAPI, blue; $n = 10$ and 6 T2DM and NDM heart sections, respectively). Scale bars = 10 μm. Data are mean ± SD.

telomerase activity, which was associated with a decreased average telomere length compared with NDM-hCSCs (Fig. 3*B*). T2DM-hCSCs expressed biomarkers of cellular senescence at significantly higher levels than NDM-hCSCs. Indeed, T2DM-hCSCs had 10 times higher levels of $p16^{INK4a}$ compared with NDM-hCSCs (Fig. 3*C*). Cytospin and immunocytochemistry at the single-cell level showed that the number of $p16^{INK4a}$-positive cells within T2DM-hCSCs was significantly higher compared with NDM-hCSCs (Fig. 3*D*).

To strengthen the reliability of p16 expression in the identification of senescence, we assessed p21 and p53

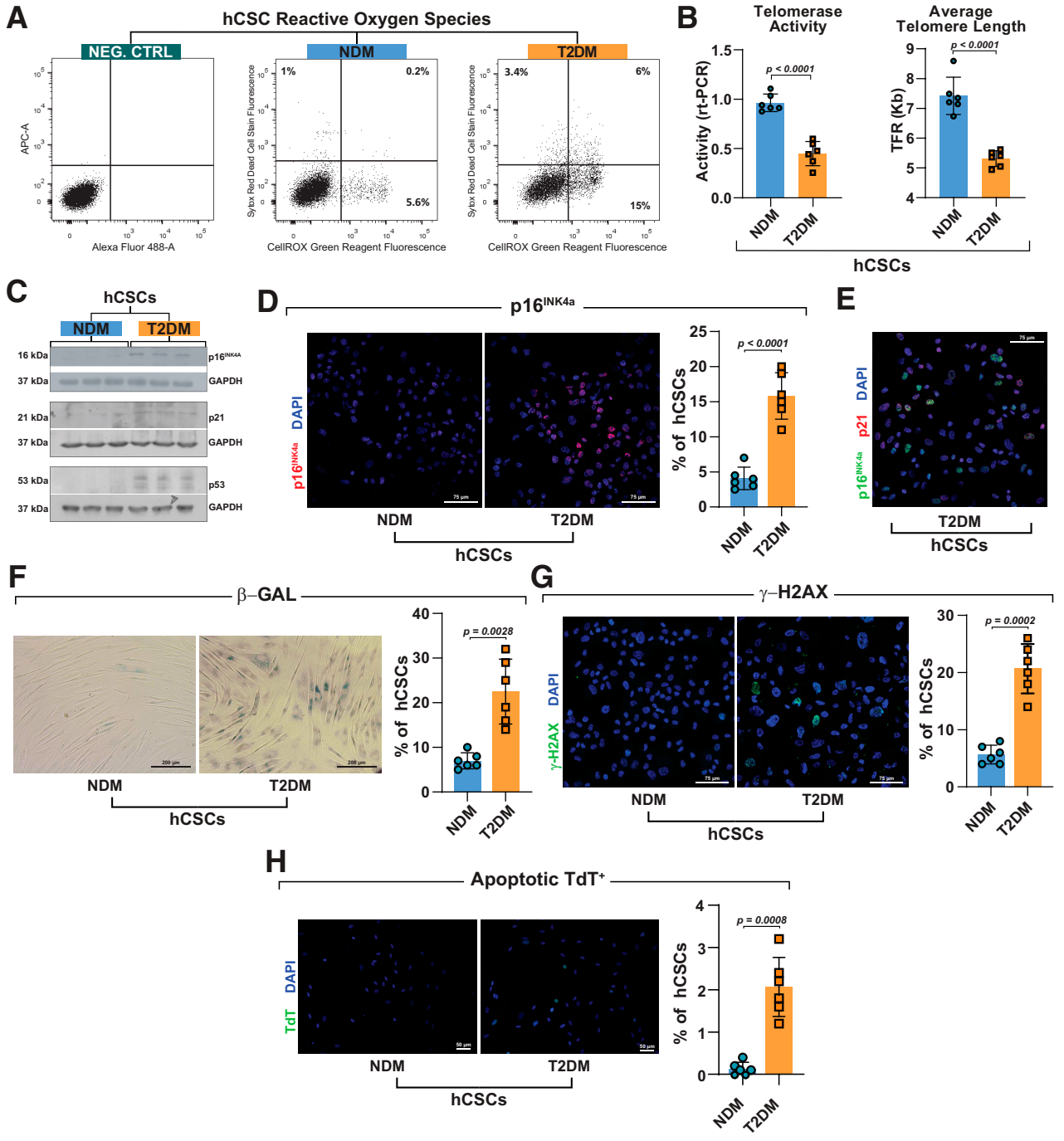

Figure 3—Phenotypic characterization of T2DM-hCSCs in vitro. *A*: Flow cytometry dot plots showing ROS in T2DM-hCSCs compared with NDM-hCSCs (representative of $n = 3$ experiments). *B*: Bar graphs showing telomerase activity and average telomere length in T2DM-hCSCs compared with NDM-hCSCs ($n = 6$ biological replicates). Data are mean ± SD. *C*: Representative Western blot showing $p16^{INK4a}$, p21, and p53 levels in T2DM-hCSCs compared with NDM-hCSCs ($n = 3$ biological replicates). *D*: Bar graph and representative confocal microscopy images from cytospin preparations showing $p16^{INK4a}$ expression (red) in T2DM-hCSCs compared with NDM-hCSCs. Scale bar = 75 μm ($n = 6$ biological replicates). *E*: Representative confocal microscopy image from cytospin preparation of T2DM-hCSCs coexpressing the senescent markers $p16^{INK4a}$ (green) and p21 (red). Scale bar = 75 μm. ($n = 6$ biological replicates). *F*: Bar graph and representative light microscopy images showing senescence-associated β-gal–positive cells (blue) in T2DM-hCSCs compared with NDM-hCSCs. Scale bar = 200 μm. ($n = 6$ biological replicates). *G* and *H*: Bar graphs and representative confocal microscopy images from cytospin preparations of c T2DM-hCSCs and NDM-hCSCs showing the expression of γ-H2AX (green) and terminal deoxynucleotidyl transferase (TdT) (green) in T2DM-hCSCs compared with NDM-hCSCs. Scale bars = 75 μm and 50 μm ($n = 6$ biological replicates). Data are mean ± SD. NEG. CTRL, negative control.

expression in hCSCs from patients with NDM and T2DM. The levels of p53, p21, and ROS were all upregulated in T2DM-hCSCs compared with NDM-hCSCs (Fig. 3*C*). Additionally, the majority of $p16^{pos}$ T2DM-hCSCs were positive for p21 (74 ± 11%) (Fig. 3*E*), lending support to the data that $p16^{pos}$ cells represent true senescent cells. Concurrently, T2DM-hCSCs showed increased senescence-associated β-galactosidase (β-gal)–positive cells in vitro (Fig. 3*F*). Furthermore, γ-H2AX expression revealed that T2DM-hCSCs accumulate significantly more DNA damage than NDM-hCSCs in vitro (Fig. 3*G*). Accordingly, T2DM-hCSCs had a significantly higher apoptotic rate compared with NDM-hCSCs (Fig. 3*H*). These data suggest that T2DM produces exaggerated oxidative stress in hCSCs that is associated with replicative senescence markers, DNA damage, reduced telomerase activity, and telomere shortening.

CSCs From Patients With T2DM Showed Impaired Cell Growth and Myogenic Differentiation Potential In Vitro

On the basis of the immunohistochemistry data showing increased $p16^{INK4a}$ expression in myocardial sections and of the in vitro data demonstrating telomerase deficit with telomere length attrition and increased p53, p21, and ROS levels, we evaluated freshly isolated T2DM-hCSCs and NDM-hCSCs for their replicative competence and growth potential in vitro. T2DM-hCSCs showed a significant decreased proliferation in vitro compared with NDM-hCSCs, as assessed either by growth curve kinetics over time or BrdU incorporation over 24 h (Fig. 4*A* and *B*). To determine whether the proliferation defect in the expansion capacity of T2DM-hCSCs was coupled with a deficit in other "stemness" capabilities, we tested these cells for their clonal amplification at the single-cell level and for their spheroid formation potential in suspension (12). At 14 days after cell deposition or plating in clonogenic or spherogenic medium, respectively, clonal efficiency and spherogenesis was 2.5-fold lower in T2DM-hCSCs compared with NDM-hCSCs (Fig. 4*C* and *D*).

These data show that T2DM increases senescence of hCSCs, affecting their expansion and clone/spheroid formation potential; thus, we tested the differentiation potential of these cells because it has been shown in different contexts that senescence and DM both affect differentiation of tissue-dependent stem/progenitor cells (19–21). Considering that myogenic differentiation is key to myocardial repair/regeneration from endogenous progenitor cells, we specifically evaluated cardiomyocyte differentiation of T2DM-hCSCs versus NDM-hCSCs grown in myogenic differentiation media (38). RT-PCR data showed that T2DM-hCSCs upregulated significantly less than NDM-hCSCs the main cardiac transcription factors (GATA-4, NKX2.5, and MEF2C) and myocyte contractile genes (*TNNT2*, *ACTC1*, *MYH6*, and *MYH7*) during myogenic differentiation induction (Fig. 4*E*). Only 24 ± 4% and 25 ± 6% of T2DM-hCSCs, compared with 52 ± 11% and 60 ± 7% of NDM-hCSCs, respectively, acquired the prototypical myocyte contractile markers cTnI and actinin by 4 weeks in culture (Fig. 4*F* and *G*). Furthermore, spontaneous beating of hCSC-derived cardiomyocytes in vitro as documentation of functional rhythmic contraction was consistently documented in NDM-hCSC–derived cardiomyocytes (Supplementary Video 1) but seldomly detected in T2DM-hCSC–derived cardiomyocytes. Overall, these data show that DM hampers hCSC biology, inducing a variety of hallmarks of senescence that contribute to the deficit of their regenerative potential.

T2DM-hCSCs Exhibit a Defined SASP

Senescent cells secrete a plethora of factors, including proinflammatory cytokines and chemokines, growth modulators, angiogenic factors, and matrix metalloproteinases (MMPs), collectively known as the SASP (8,43). The SASP constitutes a hallmark of senescent cells and mediates many of their pathophysiologic effects, such as reinforcing and spreading senescence in an autocrine and paracrine fashion (44), activating immune responses (45), hampering tissue plasticity (46), and contributing to persistent chronic inflammation (known as "inflammaging") (47). Thus, the SASP explains several of the deleterious, proaging effects of senescent cells. On the other hand, all these pathophysiologic mechanisms are equally active in DM. Therefore, we evaluated whether increased senescence markers and functional defect were associated with SASP in T2DM-hCSCs.

To this end, we obtained culture media from T2DM-hCSCs and NDM-hCSCs after 24 h in serum-free conditions to evaluate production of several SASP factors, including MMP-3, plasminogen activator inhibitor 1 (PAI-1), interleukin 6 (IL-6), IL-8, IL-1β, and granulocyte-macrophage colony-stimulating factor (GM-CSF) (Fig. 5*A* and B). Interestingly, T2DM-hCSCs secreted, respectively, 10-, 7-, 18-, 54-, and 56-fold higher amounts of IL-1A, IL-1β, IL-6, MCP-1, and IL-8 compared with NDM-hCSCs (Fig. 5*A*). Concurrently, mRNA levels of MCP-1, IGF binding protein 5 (IGFBP5), MMP-3, IL-6, CCL-11, IL-8, GM-CSF, and PAI-1 SASP factors were all increased in T2DM-hCSCs versus NDM-hCSCs (Fig. 5*B*).

We then treated for 7 days NDM-hCSCs with conditioned medium derived from T2DM-hCSCs and measured cell proliferation and senescence of the treated NDM-hCSCs. As controls, NDM-hCSCs were treated either with normal growth medium or conditioned medium from parallel cultures of NDM-hCSCs. Treatment of NDM-hCSCs with T2DM conditioned medium resulted in a decreased proliferation ($P < 0.05$) (Fig. 5*C* and *D*) and an increased proportion of senescent $p16^{INK4a}$-positive ($P < 0.05$), β-gal–positive, and γ-H2AX–positive hCSCs compared with NDM-hCSCs in unconditioned medium or conditioned medium from NDM-hCSCs (Fig. 5*E*).

Finally, we addressed whether hyperglycemia per se causes senescence, SASP, and functional impairment of hCSCs in vitro. For this aim, NDM-hCSCs were cultured for 10 days in high-glucose (30 mmol/L) or low/normal-glucose (5.5 mmol/L) conditions. High glucose significantly increased

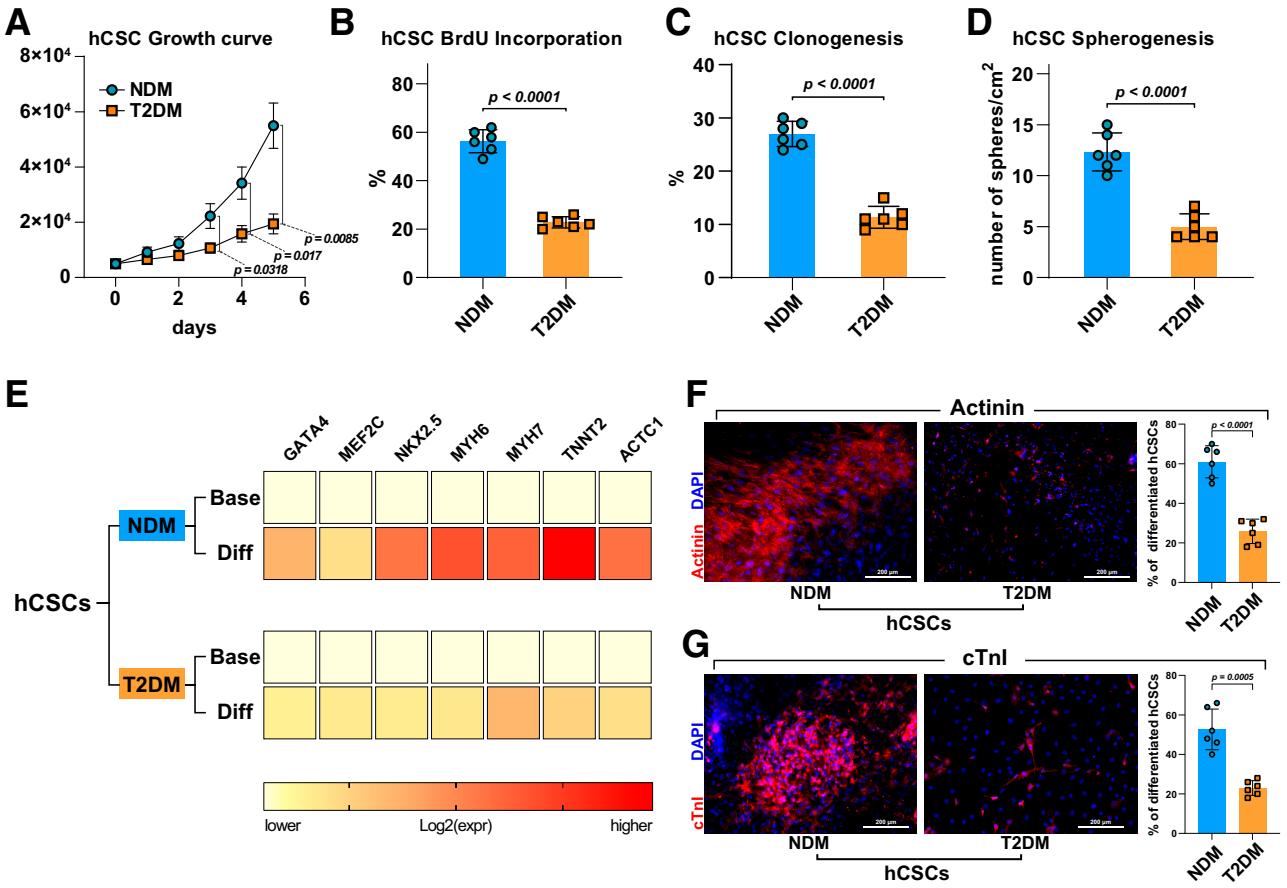

Figure 4—Impaired cell growth and myogenic differentiation potential of T2DM-hCSCs in vitro. *A*: Cell growth curve shows a decreased proliferation in vitro of T2DM-hCSCs compared with NDM-hCSCs (n = 6 biological replicates). *B–D*: Bar graphs showing BrdU incorporation, clonogenesis, and spherogenesis in T2DM-hCSCs compared with NDM-hCSCs (n = 6 biological replicates). *E*: Heat maps showing qRT-PCR analysis of the main cardiac transcription factors and myocyte contractile genes in T2DM-hCSCs compared with NDM-hCSCs after myogenic differentiation induction. Color scale indicates change in threshold cycle relative to the normalized GAPDH control (n = 3 biological replicates). *F*: Bar graph and confocal images showing actinin (red) expression levels of differentiated T2DM-hCSCs compared with NDM-hCSCs. Scale bar = 200 μm (n = 6 biological replicates). *G*: Bar graph and confocal images showing cTnI (red) expression levels of differentiated T2DM-hCSCs compared with NDM-hCSCs. Scale bar = 200 μm (n = 6 biological replicates). Data are mean ± SD. Diff, differentiated; expr, expression.

the number of $p16^{INK4a}$-positive (11 ± 5%) and β-gal–positive (16 ± 6%) NDM-hCSCs compared with low/normal glucose (1 ± 1 and 2%, respectively) (Fig. 5*F*). The latter was associated with a significant increase of SASP factors (Fig. 5*G*). Accordingly, high glucose significantly impaired expansion capacity of NDM-hCSCs (Fig. 5*H*).

These data show for the first time that the diabetic milieu, and hyperglycemia per se, induces SASP in hCSCs isolated from nonaged patients. SASP appears to negatively affect neighbor hCSCs whereby senescence begets senescence, suggesting that targeting senescent cells could improve CSC dysfunction in DM.

Senolytics Rescue the Regenerative Deficit of Diabetic hCSCs

Because senescent cells contribute to the outcome of a variety of cardiac diseases, including age-related and -unrelated cardiac diseases like anthracycline cardiotoxicity (5,48–50), much effort has been made to therapeutically target the detrimental effects of cellular senescence. Among the latter, senolytic drugs are agents that selectively induce apoptosis of only senescent cells by overriding senescent cell antiapoptotic pathways (SCAPs) specifically operative in senescent cells, although they are harmless to nonsenescent healthy cells (5). One of the most well-studied senolytic therapeutic approaches is D + Q (5). Dasatinib targets specific tyrosine kinases and other key SCAP elements. On the other hand, the flavonoid quercetin targets BCL-2 family members as well as hypoxia-inducible factor-1α and particular nodes in phosphatidylinositol 3-kinase and p21-related antiapoptotic pathways (51). Because dasatinib and quercetin target different SCAP nodes and do not target equally all senescent cell types, to extend the range of senescent cells targeted, D + Q has been used and proven effective in several mouse in vivo studies, including senescence CSCs (5), and in a first-in-man clinical trial (52).

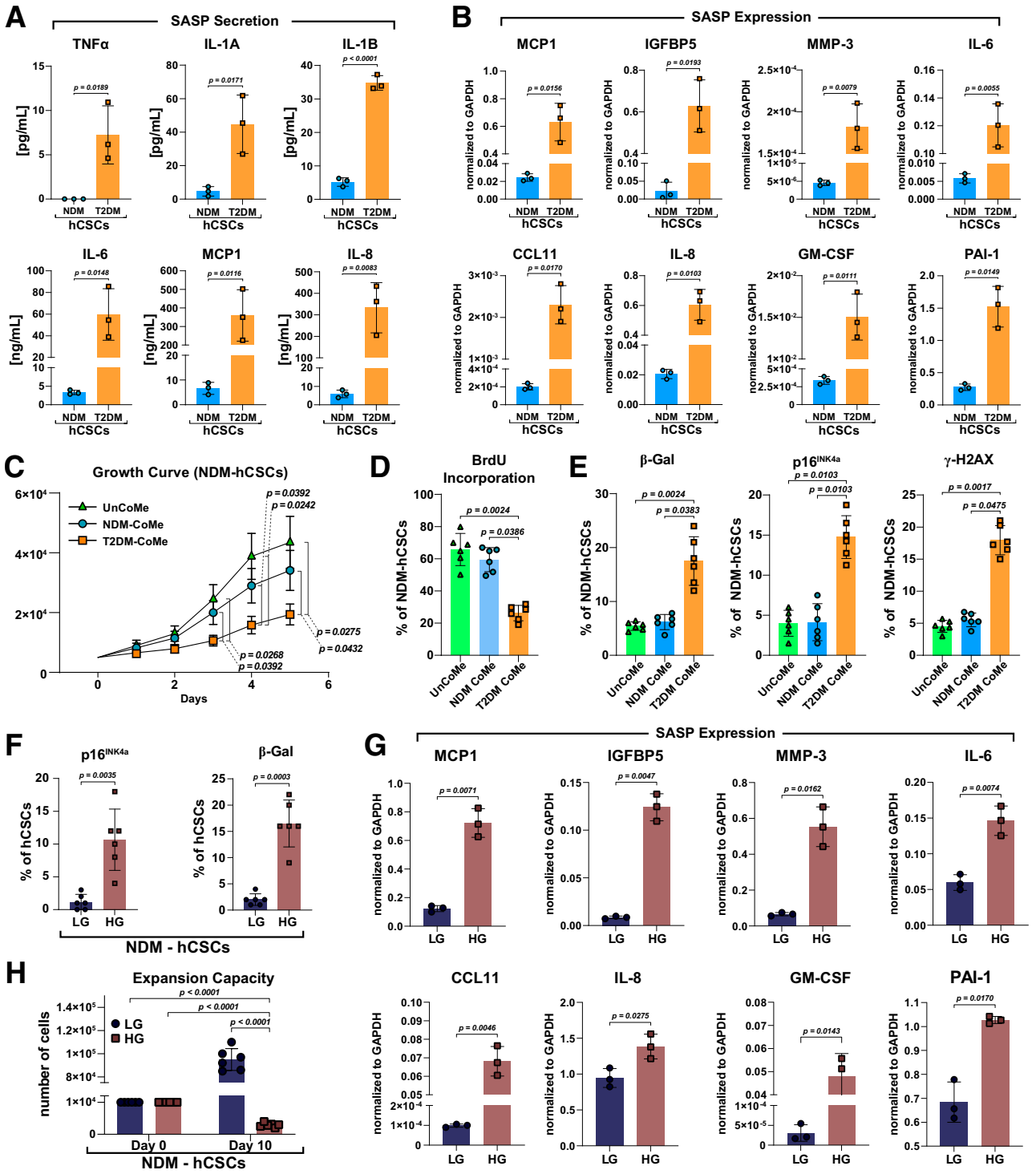

Figure 5—The SASP of T2DM-hCSCs. *A*: Bar graphs showing the SASP factor protein levels in culture media from T2DM-hCSCs and NDM-hCSCs after 24 h in serum-free conditions ($n = 3$ biological replicates). *B*: Bar graphs showing transcript SASP factor expression in T2DM-hCSCs vs. NDM-hCSCs ($n = 3$ biological replicates). *C*: Cell growth curve showing the in vitro proliferative change of NDM-hCSCs placed in conditioned medium (NSM-CoMe) derived from T2DM-hCSCs CoMe (T2DM-CoMe) compared with the NDM-hCSCs placed in unconditioned medium (UnCoMe) and NDM-hCSC CoMe ($n = 6$ biological replicates). *D*: Bar graph showing BrdU incorporation of NDM-hCSCs placed in UnCoMe, NDM-CoMe, and T2DM-CoMe ($n = 6$ biological replicates). *E*: Bar graphs showing senescent p16^{INK4a}–positive hCSCs, senescence-associated β-gal–positive hCSCs, and γ-H2AX–positive hCSCs in NDM-hCSCs treated with T2DM-CoMe compared with UnCoMe and NDM-CoMe ($n = 6$ biological replicates). *F*: Bar graphs showing the number of p16^{INK4a}– and β-gal–positive NDM-hCSCs under high-glucose (HG) conditions in vitro compared with NDM-hCSCs grown in low-glucose (LG) conditions ($n = 6$ biological replicates). *G*: Bar graphs showing transcript SASP factor expression of NDM-hCSCs under HG conditions in vitro compared with NDM-hCSCs grown in LG conditions ($n = 3$ biological replicates). *H*: Bar graphs showing expansion capacity of NDM-hCSCs under HG conditions in vitro compared with NDM-hCSCs grown in LG conditions ($n = 6$ biological replicates). Data are mean ± SD.

Thus, T2DM-hCSCs were plated in 24-well dishes at 40% confluence and left for 2 days. Then, cells were administered D + Q at a dose of 0.25 μmol/L dasatinib with 10 μmol/L quercetin. Six hours later, D + Q conditioned medium was replaced with complete fresh medium. Untreated cells served as controls. Two days later, D + Q treatment was repeated as above. Two days after, T2DM-hCSCs were analyzed for proliferation and markers of senescence, $p16^{INK4A}$, senescence-associated β-gal, and γ-H2AX. As shown in Fig. 6, D + Q treatment removed from the cell culture the typical enlarged and flattened cell morphology of senescent cells, consistent with the senolytics combination targeting and removing senescent cells (Fig. 6*A*). Concurrently, D + Q increased T2DM-hCSC proliferation as evaluated by growth curve kinetics compared with untreated control T2DM-hCSCs (Fig. 6*B*). Accordingly, D + Q significantly reduced the number of β-gal– and γ-H2AX–positive T2DM-hCSCs as well as the number of $p16^{INK4a}$ senescent cells, which almost disappeared compared with untreated T2DM-hCSCs (Fig. 6*C*–*E*). Furthermore, we determined whether D + Q would abrogate the SASP in T2DM-hCSCs. We found that the level of SASP factors secreted by T2DM-hCSCs was significantly reduced by the administration of D + Q (Fig. 6F).

Finally, considering that D + Q was able to ablate the senescent cells and the SASP from the T2DM-hCSC population, freeing the healthy nonsenescent cells, we checked whether D + Q pretreatment was able to rescue the altered myogenesis potential of T2DM-hCSCs. To that end, T2DM-hCSCs were treated or untreated with D + Q as above in growth media, and then cells were plated in bacteriological dishes for sphere formation (12). CSC-derived cardiospheres were then plated in laminin in stage-specific cardiomyogenic media (12). Interestingly, D + Q pretreatment restored the myogenic capacity of T2DM-hCSCs as, indeed, this senolytic combination significantly increased myogenic transcription factor and myogenic contractile gene expression compared with untreated cells in vitro (Fig. 6*G*). Accordingly, D + Q increased the number of T2DM-hCSC–derived cTnI-positive cardiomyocytes in differentiation media (Fig. 6*H*). Overall, these findings document that clearance of senescent cells using a combination of D + Q senolytics abrogates the SASP and restores a fully proliferative- and differentiation-competent hCSC pool in T2DM.

Senolytics Treatment In Vivo Removes Senescent CSCs and Improves Cardiac Repair and Regeneration in Diabetic Mice

The above results using human samples and cells provide a strong proof of concept for senescence and SASP as main drivers of the cardiac regeneration deficit in DM, the relevance of which was then translated and tested in a preclinical T2DM mouse model. Six-week-old C57BL/6 mice were on started a 60 kcal% HFD for 2 weeks and then on the third week, received four consecutive daily injections of low-dose STZ (40 mg/kg i.p.) (Supplementary Fig. 2*A*). These mice remained on the HFD until the completion of the study (Supplementary Fig. 2*A*). Control mice were fed NCD or HFD without STZ. Four weeks later, all animals treated with low-dose STZ and on an HFD were diabetic, showing altered fasting glycemia levels compared with control mice (Supplementary Fig. 2*B*). At this time point of the experimental design (8 weeks), 18 mice were randomly assigned to be evaluated by echocardiography, and 6 were sacrificed for cardiac histology and immunohistochemistry analysis (Supplementary Fig. 2*A*). T2DM mice had normal ejection fraction but developed diastolic dysfunction with a significant reduction in early mitral annulus tissue velocity (E′ wave) (index of LV myocardial relaxation in early diastole) and an increase in the ratio of early transmitral valve flow velocity (E wave) to E′ wave (E/E′ ratio) (an index of LV filling pressure) compared with control (NCD- and HFD-fed) mice (Fig. 7*A* and *B*), a classical feature of HF with preserved ejection fraction (53). T2DM mouse hearts had an increased production of ROS (Fig. 7C) and an increased number of myocardial (interstitial) cell nuclei positive for $p16^{INK4a}$ (2.25 ± 0.93%) compared with control mice (0.07 ± 0.02% and 0.07 ± 0.07%, respectively, for NCD and HFD) (Fig. 7D). Furthermore, compared with control mouse hearts, T2DM hearts show increased cardiomyocyte apoptosis (1.33 ± 0.4% vs. 0.01 ± 0.01 and 0.01 ± 0.01% for NCD and HFD, respectively) (Fig. 7*E*) associated with reactive myocardial interstitial fibrosis (Fig. 7*F*) and cardiomyocyte hypertrophy (Fig. 7*G*). Intriguingly, at 8 weeks of the experimental design, T2DM hearts had 6.83 ± 1.5% of their CSCs (identified as $CD45^{neg}CD31^{neg}c\text{-}kit^{pos}$ cardiac cells) positive for $p16^{INK4a}$ compared with 0.01 ± 0.01% and 0.02 ± 0.01% $p16^{INK4a}$-positive CSCs, respectively, in NCD and HFD control mice (Fig. 7*H*). These data show that diabetic status per se (independently of age and ischemia) cause myocardial cell senescence, including CSC senescence coupled with myocardial pathologic remodeling and cardiac dysfunction.

To address whether selectively eliminating senescent cells would improve cardiac function and repair in T2DM, the remaining T2DM mice ($n = 30$) with HF with preserved ejection fraction were randomized to senolytic D + Q treatment (three consecutive daily i.p. injections every week, $n = 15$) or just placebo vehicle (i.p. injection, $n = 15$) for 4 weeks. Six placebo-treated and six D + Q–treated diabetic mice were implanted subcutaneously (between the scapulae) with osmotic minipumps to systemically release BrdU (50 mg/kg/day both) for 28 days to track myocardial cell regeneration. Four weeks later, mice were assessed by echocardiography (Supplementary Fig. 2*A*), and the day after were sacrificed and their hearts processed for CSC isolation. Because of back skin pump implants, mice with BrdU pumps were not included in the echocardiography study (Supplementary Fig. 2*A*), and they were directly sacrificed at 4 weeks of treatment and processed for immunohistochemistry analysis. Echocardiography after 4 weeks

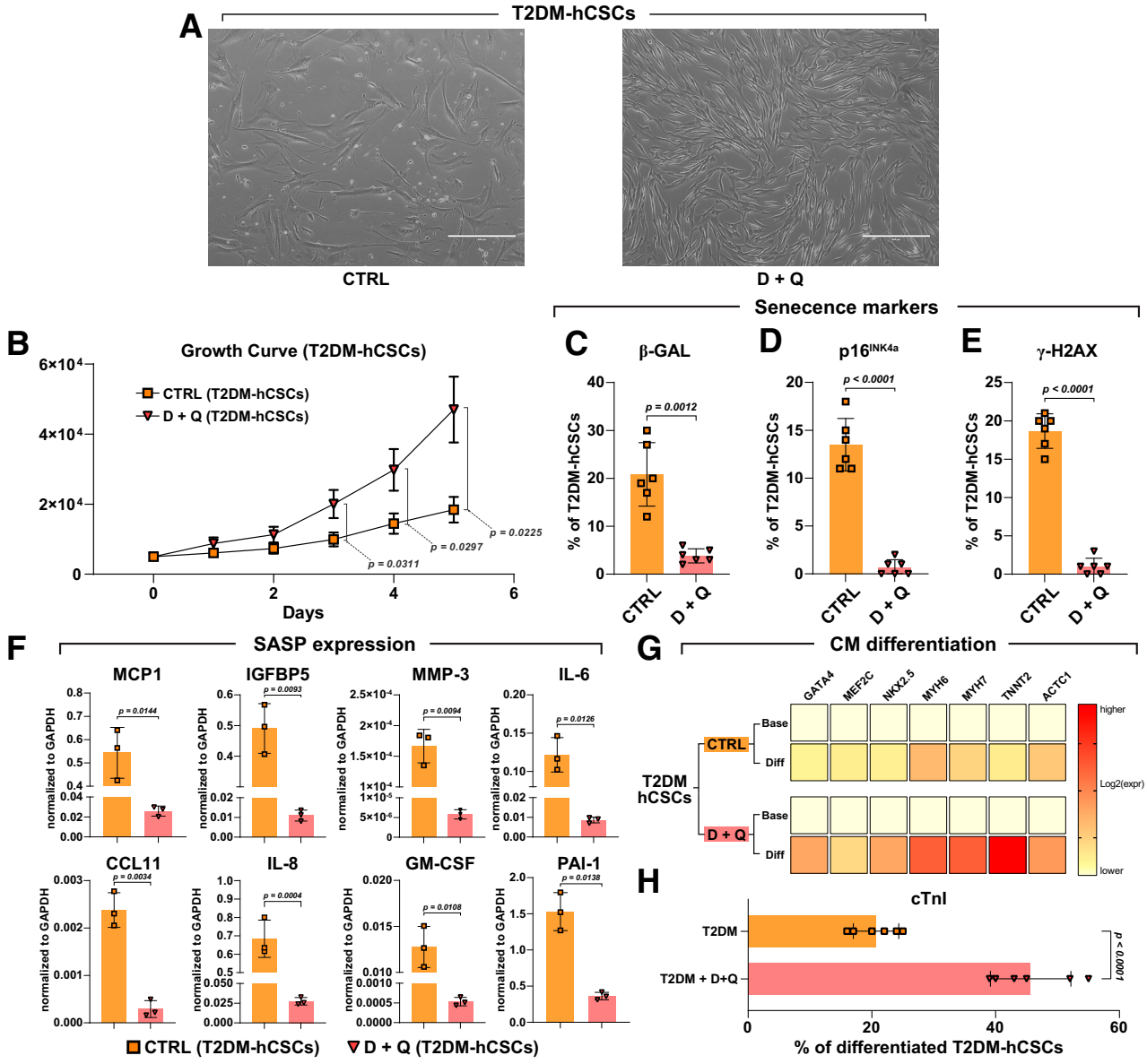

Figure 6—Senolytics ameliorates regenerative deficit of diabetic hCSCs. *A*: Light microscopy images showing that the typical enlarged and flattened morphology of senescent cells present in untreated control (CTRL) disappear in D + Q–treated T2DM-hCSCs in vitro. Scale bars = 400 μm. *B*: Cell growth curve shows the in vitro proliferation T2DM-hCSCs after D + Q treatment compared with CTRL (n = 6 biological replicates). *C–E*: Bar graphs showing the number of β-gal, p16^{INK4a} senescent cells, and γ-H2AX–positive cells in T2DM-hCSCs after D + Q treatment compared with CTRL (n = 6 biological replicates). *F*: Bar graphs showing transcript SASP factor expression in T2DM-hCSCs after D + Q treatment vs. CTRL (n = 3 biological replicates). *G*: Heat maps showing qRT-PCR analysis of the main cardiac transcription factors and myocyte contractile genes (*GATA4*, *NKX2.5*, *MEF2C*, *TNNT2*, *ACTC1*, *MYH6*, and *MYH7*) in differentiating T2DM-hCSCs after D + Q treatment vs. CTRL. Color scale indicates change in threshold cycle relative to the normalized GAPDH control (representative of n = 3 biological replicates). *H*: Bar graphs show the percentage of cTnI-expressing cells in differentiated T2DM-hCSCs after D + Q treatment vs. CTRL (n = 6 biological replicates). Data are mean ± SD. CM, cardiomyocyte; Diff, differentiated; expr, expression.

showed that vehicle-treated T2DM mice (n = 9) had persistent diastolic dysfunction compared with control mice (Fig. 8*A* and *B*). Remarkably, D + Q treatment normalized diastolic dysfunction in T2DM mice (Fig. 8*B*). D + Q treatment efficiently removed p16^{INK4a}-positive (0.5 ± 0.14%) myocardial cells compared with vehicle treatment (4.7 ± 1.3%) in T2DM mice (Supplementary Fig. 3*A*). The latter was associated with decreased cardiomyocyte apoptosis and reversal of cardiomyocyte hypertrophy in D + Q–treated versus vehicle-treated T2DM mice (Supplementary Fig. 3*B* and *C*). CSCs obtained from D + Q–treated mice showed a reduction of ROS levels compared with CSCs from control and vehicle mice (Supplementary Fig. 3*D*). Furthermore, D + Q treatment removed CSC p16^{INK4a}-positive senescent

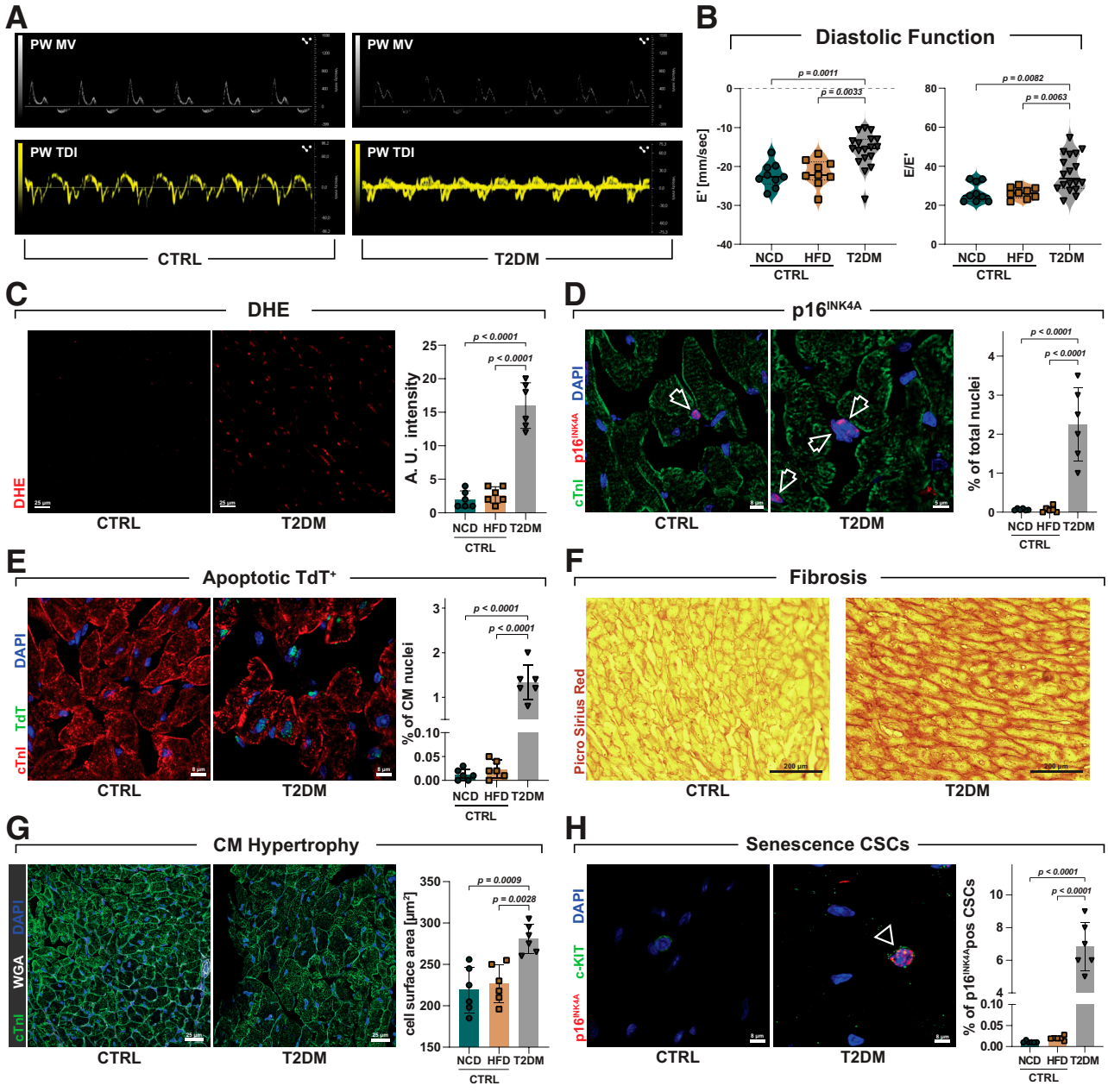

Figure 7—Diabetic status causes myocardial cell senescence with myocardial pathologic remodeling and cardiac dysfunction. *A*: Representative pulsed wave (PW) Doppler mitral velocity (MV) tracing and representative PW tissue Doppler imaging (TDI) velocity tracing of T2DM vs. control (CTRL) mice fed NCD and HFD (NCD, $n = 9$; HFD, $n = 9$; T2DM, $n = 18$). *B*: Violin plots represent cumulative E/A ratio (left) and E/E′ ratio (right) in T2DM vs. CTRL NCD and HFD mice (NCD, $n = 9$; HFD, $n = 9$; T2DM, $n = 18$). *C*: Bar graph and confocal images of dihydroethidium (DHE) detection in frozen heart sections from CTRL and T2DM mice. Scale bar = 25 μm ($n = 6$ biological replicates). *D*: Bar graph and representative confocal images showing p16^{INK4a}–positive nuclei in myocardial (interstitial) cells in T2DM mice compared with CTRL mice. Scale bar = 8 μm (left) and 5 μm (right) ($n = 6$ biological replicates). *E*: Bar graph and representative confocal images of apoptotic terminal deoxynucleotidyl transferase (TdT)–positive (green) cardiomyocyte nuclei in T2DM mice compared with CTRL mice. Scale bar = 8 μm ($n = 6$ biological replicates). *F*: Representative light microscopy of Picrosirius Red staining of T2DM mice compared with CTRL mice. Scale bar = 200 μm ($n = 6$ biological replicates). *G*: Bar graph and representative confocal images of cardiac cross section showing cardiomyocyte hypertrophy in T2DM mice compared with CTRL mice (wheat germ agglutinin [WGA] Cy5 staining, white fluorescence; cTnI, green; nuclei, DAPI blue). Scale bars = 25 μm ($n = 6$ biological replicates). *H*: Bar graph and confocal images showing the percentage of p16^{INK4a}-positive CSCs in T2DM mice compared with CTRL mice ($n = 6$ biological replicates). Data are mean ± SD.

CSCs (0.1 ± 0.07%) compared with vehicle (10.7 ± 1.5%) (Supplementary Fig. 3*E*). Intriguingly, CSCs isolated from vehicle-treated T2DM mice show a defined SASP compared with CSCs isolated from control mice (Fig. 8*C*). D + Q administration to T2DM mice significantly reduced SASP factors in CSCs (Fig. 8*C*). CSCs isolated from placebo-treated

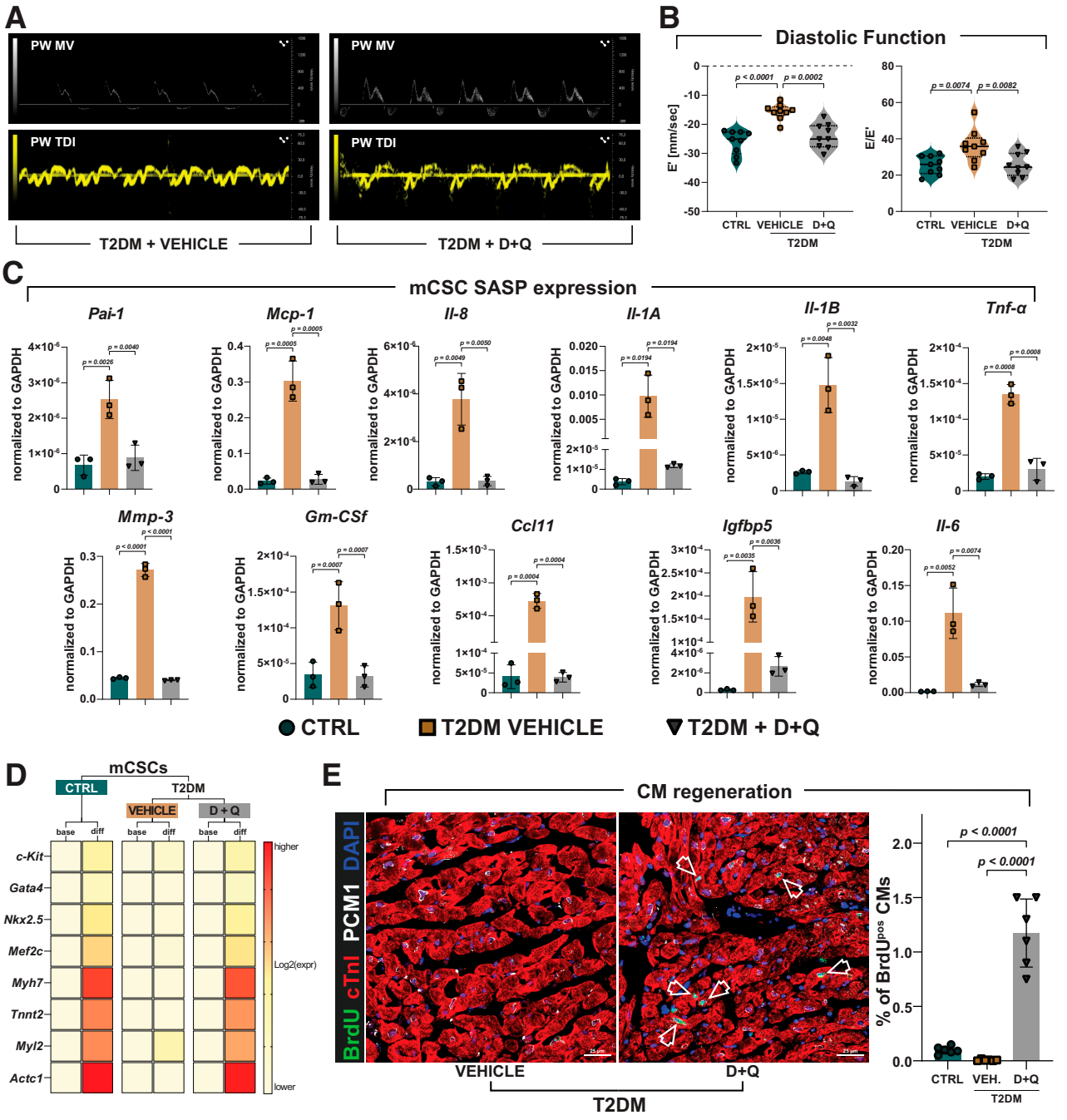

Figure 8—Senolytics treatment in vivo removes senescent CSCs and improves cardiac repair and regeneration in diabetic mice. *A*: Representative pulsed wave (PW) Doppler mitral velocity (MV) tracing and representative PW tissue Doppler imaging (TDI) velocity tracing in D + Q–treated T2DM mice compared with vehicle-treated mice (control [CTRL], $n = 9$; vehicle, $n = 9$; D + Q, $n = 9$). (Note that considering that CTRL mice fed an NCD or HFD had indistinguishable cardiac systolic and diastolic function and that their cardiac history and CSC content, phenotype, and function were comparable (data not shown), only the HFD mice are presented as the CTRL in this figure.) *B*: Violin plots represent cumulative E/A ratio (left) and E/E′ ratio (right) in D + Q–treated diabetic mice compared with vehicle-treated mice. (CTRL, $n = 9$; vehicle, $n = 9$; D + Q, $n = 9$). *C*: Bar graphs showing transcript SASP factor expression in CSCs isolated from vehicle- and D + Q–treated T2DM mice compared with CSCs isolated from CTRL mice ($n = 3$ biological replicates). *D*: Heat maps showing the myogenic differentiation of CSCs isolated from vehicle or D + Q–treated T2DM mice compared with CSCs from CTRL mice ($n = 3$ biological replicates). *E*: Bar graph and representative confocal microscopy images of BrdU-positive cardiomyocytes (arrowhead indicates BrdU-positive cardiomyocytes, green; cTnI, red; PCM1, white; nuclei, DAPI blue) in D + Q–treated T2DM mouse compared vehicle-treated mouse heart sections. Scale bar = 25 μm ($n = 6$ biological replicates). Data are mean ± SD. CM, cardiomyocyte; diff, differentiated; expr, expression; VEH., vehicle.

T2DM mice showed a reduced proliferation, clonal amplification, and myogenic differentiation in vitro compared with CSCs from control mice, consistent with T2DM imposing a senescence phenotype on CSCs (Fig. 8D and Supplementary Fig. 3*F–H*). In vivo D + Q administration eliminated the CSC senescence phenotype because CSCs isolated from D + Q–treated T2DM mice showed proliferation, clonal amplification, and myogenic differentiation potential indistinguishable from CSCs from control mice (Fig. 8*D* and Supplementary Fig. 3*F–H*). Finally, removal of both interstitial cardiac senescent cells and senescent CSCs by D + Q treatment resulted in an increased number of newly generated BrdU-positive cardiomyocytes (1.2 ± 0.31%) compared with vehicle-treated (0.007 ± 0.007%) T2DM mice (Fig. 8*E*).

Overall, these data provide further evidence that DM per se causes myocardial cell senescence independently from age, affecting CSC regenerative potential, cardiac tissue composition, and function. Accordingly, senolytics treatment efficiently eliminates senescent cells, rescuing CSC function, which results in functional myocardial repair and regeneration.

DISCUSSION

This study has several main findings. First, myocardial tissue of nonaged patients with T2DM with ischemic cardiomyopathy is characterized by an exaggerated oxidative stress targeting both cardiomyocytes and CSCs. Second, increased oxidative stress in the myocardium of nonaged patients with T2DM is associated with an increased number of senescent and dysfunctional T2DM-hCSCs as shown by increased $p16^{INK4a}$, p53, and p21 expression, reduced telomerase activity and telomere length, reduced proliferation, clonogenesis/spherogenesis, and myogenic differentiation. Third, T2DM-hCSCs from nonaged patients show an SASP, as demonstrated by increased secretion of several SASP factors, including MMP-3, PAI-1, IL-6, IL-8, IL-1β, and GM-CSF. Fourth, a combination of two senolytics, dasatinib and quercetin, clear senescent T2DM-hCSCs, restoring expansion and myogenic differentiation capacities of the remaining diabetic hCSC pool. Fifth, diabetic cardiomyopathy in young mice, independently of age and ischemia, causes myocardial cell senescence, affecting CSC regenerative potential and cardiac tissue composition and function. Finally, D + Q treatment in vivo removes senescent CSCs and improves cardiac repair, regeneration, and function in diabetic mice.

T2DM is a preconditioning and powerful driver of organismal aging (54). The biological foundations of aging primarily involve cellular senescence, and T2DM is plethoric in senescence-driving factors (54). An intense debate exists about whether senescence precedes or follows the onset of perpetual inflammation and insulin resistance in T2DM (55). Independently from "whom precedes who," patients with DM experience an obvious accelerated aging process that increases their susceptibility to morbidity and earlier mortality mainly from cardiovascular disease (56,57).

Adult tissue-specific stem cells are multipotent cells that are considered a lifelong cellular reservoir to ensure the continuous generation, replacement, and restitution of multiple tissue lineages (57,58). However, during aging, these cells also undergo some detrimental changes, such as alterations in the microenvironment, a decline in the regenerative capacity, and loss of function. Therefore, aging has been linked to tissue-specific adult stem cell exhaustion (35). Converging evidence conclusively demonstrated how toxic high-glucose load may be for survival, differentiation plasticity, and regenerative competence for various stem cell lineages (53,59–63). The self-sustaining vicious circle of hyperglycemia/mitochondrial dysfunction/oxidative stress appears as a master driver to adult stem cell senescence (64). Accordingly, the diabetic prooxidative environment is a major contributing factor for premature adult stem cell senescence and functional deficit (53,64–68). Therefore, aging and T2DM drive adult stem cell senescence and regenerative deficit, and, conversely, adult stem cell senescence and regenerative deficit drive the progressive pathology in aging and DM.

Like other tissue-specific adult stem/progenitor cells, the CSCs are not immortal (16). They undergo cellular senescence characterized by increased ROS production and oxidative stress and loss of telomere/telomerase integrity in response to a variety of physiologic and pathologic demands with aging (16). Nevertheless, the old myocardium preserves an endogenous functionally competent CSC cohort, which appears to be resistant to the senescent phenotype that occurs with aging (16). The latter demonstrates the phenomenon of CSC aging as a result of a stochastic process whereby targeting the senescent cells would benefit the recovery of a healthy CSC cohort (16). Concurrently, T2DM impairs the in vitro proliferative and differentiation potential of hCSCs, worsening their senescence phenotype compared with CSCs from patients with NDM and ischemia (22). Additionally, miR-34a is significantly upregulated while SIRT1 is downregulated in adult CSCs harvested from patients with T2DM, which is associated with a higher proapoptotic caspase-3/7 activity (69). In all these studies, however, researchers isolated hCSCs from older (>65 years of age) patients with DM, which could not clearly distinguish the role of age from DM on hCSC function. On the other hand, in an animal model of insulin-dependent DM in young mice, the myocardial accumulation of ROS drove CSC senescence through the expression of p53 and $p16^{INK4a}$ proteins and telomere erosion (31). The $p66^{shc}$ knockout inhibited CSC senescence and death, preventing the senescent phenotype and the development of cardiac failure by T2DM (31). Additionally, DM persistently decreases the ability of isolated CSCs from young male mice to proliferate, survive oxidative insults, and differentiate, which can be explained at least in part by an uncoupling of biosynthetic glucose

metabolism pathways (69). Altogether, these data lead us to postulate the tantalizing hypothesis that the premature cellular senescence of resident CSCs underpins the development of diabetic heart disease (10).

In the current study, we provide evidence of the existence of premature senescence of hCSCs in T2DM, demonstrating its functional relevance in the regenerative biology of these cells. Indeed, the elimination of senescent cells by senolytic D + Q treatment rescued the expansion and myogenic capacity of T2DM-hCSCs. Therefore, these data suggest that eliminating senescent hCSCs by senolytic therapy in vivo could be a therapeutic strategy to prevent CSC dysfunction, even at early stages of diabetic disease.

Our findings in hCSCs are clearly hampered by the difficulty and limitation of working with samples of human tissue, which makes these data mainly descriptive and hypothesis generating while falling short of being able to establish direct cause-and-effect relationships. Furthermore, to separate the effects of old age and diabetes on senescence, we chose an age cutoff of <65 years to define nonaged patients, which might be seen as an arbitrary threshold when considering that the World Health Organization uses 60 years as the age cutoff for predicting the shift in distribution of a country's population toward older ages, known as population aging. Yet, old age in human beings is inconsistently defined from the standpoints of biology, demography (conditions of mortality and morbidity), employment and retirement, and sociology. For example, in high-income countries, setting 60 years as the threshold for aging is unrealistic because >30% of the relative population is already >60 years old. Furthermore, several cardiovascular risk scores (and the CHA_2DS_2-VASc [congestive HF, hypertension, age ≥75 years, DM, stroke or transient ischemic attack, vascular disease, age 65–74 years, sex category] score for thromboembolism in atrial fibrillation) use 65 years to define aged/older people. Therefore, despite being imperfect, we chose this age cutoff. As a further limitation of the study on human samples, we could not fully extrapolate the role of ischemic damage to the observed effects of T2DM on hCSC senescence in vivo. Indeed, DM is known to determine more intense microvascular ischemia and arterial dysfunction, which may have affected the status and function of hCSCs. Concurrently, short leukocyte telomere length has been associated with plaque instability (70) and changes in several hemodynamic parameters such as impaired pressure-diameter relation and increased pulse pressure and pulse wave velocity, which are indicative of increased arterial stiffness (71–73). When considering that telomere length shortening can be both a cause and an effect of vascular disease, it is then possible that hCSC senescence within the myocardial microenvironment might be influenced by telomere dysregulation in the arterial system affected by DM. Despite all the above, it should be noted that isolated T2DM-hCSCs and NDM-hCSCs were obtained from right atrial tissue that was not ischemic. Moreover, according to the "oxygen stem cell paradigm," adult stem cells are kept in niches with a very low oxygen concentration (15). Relevant to our study, it already has been shown that hypoxia (0.5% oxygen) reduces hCSC senescence and promotes CSC quiescence, while long-term exposure to low oxygen levels (1%) increases hCSC proliferation, shifting CSC secretome to a more anti-inflammatory profile (74). Finally, the diabetic milieu is a multifactorial environment constituting several elements (e.g., high glucose, advanced glycosylation end products, angiotensin, oxidative stress) that induce the expression of chemokines and adhesion molecules activating an inflammatory phenomenon linked to cell senescence (3). All these elements, therefore, also could be responsible for the senescent cells in the myocardium of patients with DM.

Considering all the above limitations, through a reverse translational approach, we tested in a preclinical mouse model of T2DM the proof of concept provided by the human study that senescence and SASP are mechanistically linked to the cardiac regeneration defect of the human diabetic myocardium, independently of age and ischemia. The murine data conclusively show that the working hypothesis generated by the in vitro data on hCSC regenerative biology is indeed correct. T2DM in young mice causes CSC senescence and SASP, ensuing in a detrimental cardiac remodeling characterized by cardiomyocyte death and reduced regeneration owing to HF with preserved ejection fraction characterized by short- and midterm diastolic dysfunction. Efficient removal of senescent cardiac cells, including senescent CSCs, by systemic senolytic D + Q treatment restores CSC regenerative potential and cardiomyocyte regeneration, normalizing cardiac function in T2DM mice.

In conclusion, DM hampers, independently of age, CSC biology, inducing cellular senescence and SASP that contribute to a significant deficit of the regenerative potential and, in particular, ability of CSCs to differentiate in new cardiomyocytes. Clearance of senescent cells by senolytics abrogates the SASP and restores a fully proliferative- and differentiation-competent hCSC pool in T2DM. Therefore, senolytics may represent a potential therapeutic approach to prevent or treat the reduced regenerative potential of the diabetic heart.

Funding. This research was funded by Ministero dell'Instruzione, dell'Università e della Ricerca grants PRIN2015ZTT5KB_004, PRIN2017NKB2N4_005, and PON-AIM–1829805-2.

Duality of Interest. No potential conflicts of interest relevant to this article were reported.

Author Contributions. F.M., M.Sc., N.S., L.S., C.M., D.C., and M.G. contributed to the data acquisition and analysis. M.T., D.F., F.C.S, P.M., A.D.A., K.U., D.T., and E.C. contributed to the data interpretation. A.D.A., G.M.E.-H., K.U., D.T., and E.C. designed the study. G.M.E.-H., M.Sa., M.R., and F.R. provided critical feedback and helped to shape the research, analysis, and manuscript. K.U., B.N-G., D.T., and E.C. wrote the original draft and edited the manuscript. K.U., D.T., and E.C. contributed to the conceptualization. All the authors approved the final version of this manuscript. D.T. and E.C. are the guarantors of this work and, as such, had full access to all the

data in the study and take responsibility for the integrity of the data and the accuracy of the data analysis.

References

1. Dunlay SM, Givertz MM, Aguilar D, et al.; American Heart Association Heart Failure and Transplantation Committee of the Council on Clinical Cardiology; Council on Cardiovascular and Stroke Nursing and the Heart Failure Society of America. Type 2 diabetes mellitus and heart failure: a scientific statement from the American Heart Association and the Heart Failure Society of America: This statement does not represent an update of the 2017 ACC/AHA/HFSA heart failure guideline update. Circulation 2019;140:e294–e324
2. Gude NA, Broughton KM, Firouzi F, Sussman MA. Cardiac ageing: extrinsic and intrinsic factors in cellular renewal and senescence. Nat Rev Cardiol 2018;15:523–542
3. Halim M, Halim A. The effects of inflammation, aging and oxidative stress on the pathogenesis of diabetes mellitus (type 2 diabetes). Diabetes Metab Syndr 2019;13:1165–1172
4. van Deursen JM. The role of senescent cells in ageing. Nature 2014;509:439–446
5. Lewis-McDougall FC, Ruchaya PJ, Domenjo-Vila E, et al. Aged-senescent cells contribute to impaired heart regeneration. Aging Cell 2019;18:e12931
6. Tchkonia T, Zhu Y, van Deursen J, Campisi J, Kirkland JL. Cellular senescence and the senescent secretory phenotype: therapeutic opportunities. J Clin Invest 2013;123:966–972
7. Xu M, Palmer AK, Ding H, et al. Targeting senescent cells enhances adipogenesis and metabolic function in old age. eLife 2015;4:e12997
8. Acosta JC, Banito A, Wuestefeld T, et al. A complex secretory program orchestrated by the inflammasome controls paracrine senescence. Nat Cell Biol 2013;15:978–990
9. Shakeri H, Lemmens K, Gevaert AB, De Meyer GRY, Segers VFM. Cellular senescence links aging and diabetes in cardiovascular disease. Am J Physiol Heart Circ Physiol 2018;315:H448–H462
10. Cianflone E, Torella M, Biamonte F, et al. Targeting cardiac stem cell senescence to treat cardiac aging and disease. Cells 2020;9:1558
11. Cianflone E, Aquila I, Scalise M, et al. Molecular basis of functional myogenic specification of bona fide multipotent adult cardiac stem cells. Cell Cycle 2018;17:927–946
12. Scalise M, Torella M, Marino F, et al. Atrial myxomas arise from multipotent cardiac stem cells. Eur Heart J 2020;41:4332–4345
13. Scalise M, Marino F, Cianflone E, et al. Heterogeneity of adult cardiac stem cells. Adv Exp Med Biol 2019;1169:141–178
14. Di Siena S, Gimmelli R, Nori SL, et al. Activated c-Kit receptor in the heart promotes cardiac repair and regeneration after injury. Cell Death Dis 2016;7:e2317
15. Vicinanza C, Aquila I, Cianflone E, et al. Kit^{cre} knock-in mice fail to fate-map cardiac stem cells. Nature 2018;555:E1–E5
16. Cianflone E, Torella M, Chimenti C, et al. Adult cardiac stem cell aging: a reversible stochastic phenomenon? Oxid Med Cell Longev 2019;2019:5813147
17. Marino F, Scalise M, Cianflone E, et al. Role of c-Kit in myocardial regeneration and aging. Front Endocrinol (Lausanne) 2019;10:371
18. Tchkonia T, Kirkland JL. Aging, cell senescence, and chronic disease: emerging therapeutic strategies. JAMA 2018;320:1319–1320
19. Zhang X, Meng K, Pu Y, Wang C, Chen Y, Wang L. Hyperglycemia altered the fate of cardiac stem cells to adipogenesis through inhibiting the β-catenin/TCF-4 pathway. Cell Physiol Biochem 2018;49:2254–2263
20. She T, Wang X, Gan Y, et al. Hyperglycemia suppresses cardiac stem cell homing to peri-infarcted myocardium via regulation of ERK1/2 and p38 MAPK activities. Int J Mol Med 2012;30:1313–1320
21. Molgat AS, Tilokee EL, Rafatian G, et al. Hyperglycemia inhibits cardiac stem cell-mediated cardiac repair and angiogenic capacity. Circulation 2014;130(Suppl. 1):S70–S76
22. Vecellio M, Spallotta F, Nanni S, et al. The histone acetylase activator pentadecylidenemalonate 1b rescues proliferation and differentiation in the human cardiac mesenchymal cells of type 2 diabetic patients. Diabetes 2014;63:2132–2147
23. Torella D, Ellison GM, Torella M, et al. Carbonic anhydrase activation is associated with worsened pathological remodeling in human ischemic diabetic cardiomyopathy. J Am Heart Assoc 2014;3:e000434
24. Luo J, Quan J, Tsai J, et al. Nongenetic mouse models of non-insulin-dependent diabetes mellitus. Metabolism 1998;47:663–668
25. Tate M, Prakoso D, Willis AM, et al. Characterising an alternative murine model of diabetic cardiomyopathy. Front Physiol 2019;10:1395
26. Aquila I, Cianflone E, Scalise M, et al. c-kit haploinsufficiency impairs adult cardiac stem cell growth, myogenicity and myocardial regeneration. Cell Death Dis 2019;10:436
27. Scalise M, Marino F, Salerno L, et al. In vitro CSC-derived cardiomyocytes exhibit the typical microRNA-mRNA blueprint of endogenous cardiomyocytes. Commun Biol 2021;4:1146
28. Xin H. Telomeric repeat amplification protocol: measuring the activity of the telomerase. Methods Mol Biol 2011;735:107–111
29. Accattato F, Greco M, Pullano SA, et al. Effects of acute physical exercise on oxidative stress and inflammatory status in young, sedentary obese subjects. PLoS One 2017;12:e0178900
30. Pham-Huy LA, He H, Pham-Huy C. Free radicals, antioxidants in disease and health. Int J Biomed Sci 2008;4:89–96
31. Rota M, LeCapitaine N, Hosoda T, et al. Diabetes promotes cardiac stem cell aging and heart failure, which are prevented by deletion of the p66shc gene. Circ Res 2006;99:42–52
32. Coluzzi E, Colamartino M, Cozzi R, et al. Oxidative stress induces persistent telomeric DNA damage responsible for nuclear morphology change in mammalian cells. PLoS One 2014;9:e110963
33. Rodier F, Muñoz DP, Teachenor R, et al. DNA-SCARS: distinct nuclear structures that sustain damage-induced senescence growth arrest and infla mmatory cytokine secretion. J Cell Sci 2011;124:68–81
34. Gorgoulis V, Adams PD, Alimonti A, et al. Cellular senescence: defining a path forward. Cell 2019;179:813–827
35. Oh J, Lee YD, Wagers AJ. Stem cell aging: mechanisms, regulators and therapeutic opportunities. Nat Med 2014;20:870–880
36. McConnell BB, Gregory FJ, Stott FJ, Hara E, Peters G. Induced expression f p16(INK4a) inhibits both CDK4- and CDK2-associated kinase activity by reassortment of cyclin-CDK-inhibitor complexes. Mol Cell Biol 1999;19:1981–1989
37. Jeyapalan JC, Sedivy JM. Cellular senescence and organismal aging. Mech Ageing Dev 2008;129:467–474
38. Kirkland JL, Hollenberg CH, Gillon WS. Age, anatomic site, and the replication and differentiation of adipocyte precursors. Am J Physiol 1990;258: C206–C210
39. Sharpless NE, DePinho RA. How stem cells age and why this makes us grow old. Nat Rev Mol Cell Biol 2007;8:703–713
40. Liu JY, Souroullas GP, Diekman BO, et al. Cells exhibiting strong $p16^{INK4a}$ promoter activation in vivo display features of senescence. Proc Natl Acad Sci U S A 2019;116:2603–2611
41. Vicinanza C, Aquila I, Scalise M, et al. Adult cardiac stem cells are multipotent and robustly myogenic: c-kit expression is necessary but not sufficient for their identification. Cell Death Differ 2017;24:2101–2116
42. Smith AJ, Lewis FC, Aquila I, et al. Isolation and characterization of resident endogenous c-Kit+ cardiac stem cells from the adult mouse and rat heart. Nat Protoc 2014;9:1662–1681
43. Kumari R, Jat P. Mechanisms of cellular senescence: cell cycle arrest and senescence associated secretory phenotype. Front Cell Dev Biol 2021;9:645593
44. Hoare M, Narita M. Transmitting senescence to the cell neighbourhood. Nat Cell Biol 2013;15:887–889

45. Burton DGA, Stolzing A. Cellular senescence: immunosurveillance and future immunotherapy. Ageing Res Rev 2018;43:17–25
46. Ritschka B, Storer M, Mas A, et al. The senescence-associated secretory phenotype induces cellular plasticity and tissue regeneration. Genes Dev 2017;31:172–183
47. Franceschi C, Garagnani P, Vitale G, Capri M, Salvioli S. Inflammaging and 'garb-aging'. Trends Endocrinol Metab 2017;28:199–212
48. Carresi C, Musolino V, Gliozzi M, et al. Anti-oxidant effect of bergamot polyphenolic fraction counteracts doxorubicin-induced cardiomyopathy: role of autophagy and c-kit^{pos}CD45^{neg}CD31^{neg} cardiac stem cell activation. J Mol Cell Cardiol 2018;119:10–18
49. Piegari E, De Angelis A, Cappetta D, et al. Doxorubicin induces senescence and impairs function of human cardiac progenitor cells. Basic Res Cardiol 2013;108:334
50. Cappetta D, De Angelis A, Sapio L, et al. Oxidative stress and cellular response to doxorubicin: a common factor in the complex milieu of anthracycline cardiotoxicity. Oxid Med Cell Longev 2017;2017:1521020
51. Wissler Gerdes EO, Zhu Y, Tchkonia T, Kirkland JL. Discovery, development, and future application of senolytics: theories and predictions. FEBS J 2020;287:2418–2427
52. Hickson LJ, Langhi Prata LGP, Bobart SA, et al. Senolytics decrease senescent cells in humans: preliminary report from a clinical trial of dasatinib plus quercetin in individuals with diabetic kidney disease. EBioMedicine 2019;47:446–456
53. McHugh K, DeVore AD, Wu J, et al. Heart failure with preserved ejection fraction and diabetes: JACC state-of-the-art review. J Am Coll Cardiol 2019;73:602–611
54. Berlanga-Acosta JA, Guillén-Nieto GE, Rodríguez-Rodríguez N, et al. Cellular senescence as the pathogenic hub of diabetes-related wound chronicity. Front Endocrinol (Lausanne) 2020;11:573032
55. Prattichizzo F, De Nigris V, La Sala L, Procopio AD, Olivieri F, Ceriello A. "Inflammaging" as a druggable target: a senescence-associated secretory phenotype-centered view of Type 2 diabetes. Oxid Med Cell Longev 2016;2016:1810327
56. Perkisas S, Vandewoude M. Where frailty meets diabetes. Diabetes Metab Res Rev 2016;32(Suppl. 1):261–267
57. Wright AK, Kontopantelis E, Emsley R, et al. Life expectancy and cause-specific mortality in type 2 diabetes: a population-based cohort study quantifying relationships in ethnic subgroups. Diabetes Care 2017;40:338–345
58. Andrzejewska A, Lukomska B, Janowski M. Concise review: mesenchymal stem cells: from roots to boost. Stem Cells 2019;37:855–864
59. Yang G, Jia Y, Li C, Cheng Q, Yue W, Pei X. Hyperglycemic stress impairs the stemness capacity of kidney stem cells in rats. PLoS One 2015;10:e0139607
60. Dienelt A, zur Nieden NI. Hyperglycemia impairs skeletogenesis from embryonic stem cells by affecting osteoblast and osteoclast differentiation. Stem Cells Dev 2011;20:465–474
61. Xu W, Yu W, Gao H, Wang L, Liu X, Wang Y. Effects of high glucose and high lipid on proliferation and apoptosis of human umbilical cord mensenchymal stem cells. Chin J Tissue Eng Res. 2012;16:5001–5005
62. Kränkel N, Adams V, Linke A, et al. Hyperglycemia reduces survival and impairs function of circulating blood-derived progenitor cells. Arterioscler Thromb Vasc Biol 2005;25:698–703
63. Torella D, Iaconetti C, Tarallo R, et al. miRNA regulation of the hyperproliferative phenotype of vascular smooth muscle cells in diabetes. Diabetes 2018;67:2554–2568
64. Vono R, Jover Garcia E, Spinetti G, Madeddu P. Oxidative stress in mesenchymal stem cell senescence: regulation by coding and noncoding RNAs. Antioxid Redox Signal 2018;29:864–879
65. Cassidy FC, Shortiss C, Murphy CG, et al. Impact of type 2 diabetes mellitus on human bone marrow stromal cell number and phenotypic characteristics. Int J Mol Sci 2020;21:2476
66. Ko KI, Coimbra LS, Tian C, et al. Diabetes reduces mesenchymal stem cells in fracture healing through a TNFα-mediated mechanism. Diabetologia 2015;58:633–642
67. van de Vyver M, Niesler C, Myburgh KH, Ferris WF. Delayed wound healing and dysregulation of IL6/STAT3 signalling in MSCs derived from pre-diabetic obese mice. Mol Cell Endocrinol 2016;426:1–10
68. Lu H, Wu X, Wang Z, et al. Erythropoietin-activated mesenchymal stem cells promote healing ulcers by improving microenvironment. J Surg Res 2016;205:464–473
69. Fomison-Nurse I, Saw EEL, Gandhi S, et al. Diabetes induces the activation of pro-ageing miR-34a in the heart, but has differential effects on cardiomyocytes and cardiac progenitor cells. Cell Death Differ 2018; 25:1336–1349
70. De Meyer T, Nawrot T, Bekaert S, De Buyzere ML, Rietzschel ER, Andrés V. Telomere length as cardiovascular aging biomarker: JACC review topic of the week. J Am Coll Cardiol 2018;72:805–813
71. Peng H, Zhu Y, Yeh F, et al. Impact of biological aging on arterial aging in American Indians: findings from the Strong Heart Family Study. Aging (Albany NY) 2016;8:1583–1592
72. Benetos A, Okuda K, Lajemi M, et al. Telomere length as an indicator of biological aging: the gender effect and relation with pulse pressure and pulse wave velocity. Hypertension 2001;37:381–385
73. Honkonen M, Vääräniemi K, Saijonmaa O, et al. Leukocyte telomere length is inversely associated with arterial wave reflection in 566 normo tensive and never-treated hypertensive subjects. Aging (Albany NY) 2020; 12:12376–12392
74. Bellio MA, Rodrigues CO, Landin AM, et al. Physiological and hypoxic oxygen concentration differentially regulates human c-Kit+ cardiac stem cell proliferation and migration. Am J Physiol Heart Circ Physiol 2016;311: H1509–H1519